Structural Reconstruction Modulated Physical Properties of Titanium Oxide at The Monolayer Limit

Tong Yang[1, 2, †], Ke Yang[2,3, †], Tao Zhu[4, 5, †], Ting Ting Song[6], Tian Bao[1], Jun Zhou[7], Shi Jie Wang[7], Yunjiang Jin[8, *], Martin Callsen[9, *] and Ming Yang[2, *]

[1]State Key Laboratory of Advanced Technology for Float Glass, CNBM Research Institute for Advanced Glass Materials Group Co., Ltd, Bendu 233000, China

[2] Department of Applied Physics, The Hong Kong Polytechnic University, Hung Hom, Hong Kong SAR, China.

[3] Department of Computing, The Hong Kong Polytechnic University, Hung Hom, Hong Kong SAR, China

[4] School of Electronic and Information Engineering, Tiangong University, Tianjin 300387, China

[5] Beijing National Laboratory for Condensed Matter Physics, Institute of Physics, Chinese Academy of Sciences, Beijing 100190, China

[6] College of Physics and Space Science, China West Normal University, Nanchong 637002, China

[7] Institute of Materials Research and Engineering, A∗STAR, 2 Fusionopolis Way, Singapore 138634, Singapore.

[8] School of Electronics and Information Technology, State Key Laboratory of Optoelectronic Materials and Technologies, Sun Yat-Sen University, 510006, China

[9] Institute of Atomic and Molecular Sciences, Academia Sinica, Taipei 10617, Taiwan

[†] These authors contribute equally to this work.

Authors to whom correspondence should be addressed: M. Y. (kevin.m.yang@polyu.edu.hk); M. C. (mcallsen@gate.sinica.edu.tw); Y. J. J.(jinyj5@mail.sysu.edu.cn)

Keywords: Titanium Dioxide Monolayer, Intrinsic Flat Band, Small Polaron, Exciton, First-principles Calculations, Tight Binding Modelling

Abstract

To suppress surface dangling bonds, monolayer oxides derived from non-layered bulks usually undergo a pronounced structural reconstruction. It remains challenging to resolve these structural reconstructions and the induced distinct modulation of intrinsic properties. In this study, the structural reconstruction modulated electronic, polaronic, and exitonic properties of a non-layered oxide at the monolayer limit are unravelled. Based on first-principles calculations and tight-binding simulations for a stable titanium dioxide (TiO_2) monolayer, we show that its distinct surface Kagome sublattices host a topologically nontrivial flat band at the valence band edge. The strong electron-hole interaction in this monolayer oxide gives rise to a large exciton binding energy of around 2.49 eV. Interestingly, the monolayer TiO_2 also exhibits strong electron-lattice coupling, which favours the formation of small electron polarons and thus greatly reduces its band gap energy into the visible light range. This work could be useful to understand the structural reconstruction induced modulation of exotic physical and chemical properties for a broad range of non-layered oxides at the monolayer limit.

Introduction

The delamination of graphene has aroused enormous interest in two-dimensional (2D) materials with stunning physical and chemical properties.[1-4] Many 2D materials, such as hexagonal boron nitride (*h*-BN),[5] transition metal dichalcogenides (TMDs),[6, 7] group III and group IV metal chalcogenides,[8-10] and phosphorene,[11] have been exfoliated from van der Waals (vdW) layered crystals. These 2D materials resemble the constituent single layer of their parent bulks, since they are held together by weak vdW interactions. However, this is not the case for non-layered oxides.[12-23] When strong metal-oxygen bonds are cleaved, substantial structural reconstructions have been noted in these oxide monolayers in order to minimize the surface polarization or dangling bonds.[14-16] The significant structural reconstruction makes it challenging to theoretically predict the non-layered oxide structures at the monolayer limit or resolve experimentally grown oxide monolayers. A model example is the titania (TiO_2) monolayer. Although a TiO_2 2D phase has been realized on the rutile-TiO_2 (011) surface[17] for more than a decade, its ground state structure in the monolayer limit is still under debate.[24-26]

Significant structural reconstructions at the monolayer limit could simultaneously lead to drastic modulation of the intrinsic properties of non-layered oxides.[13, 23, 27-29] For examples, the dielectric constant of 2D hafnium dioxide (HfO_2) is about 50% higher than that of its bulk counterpart[13, 27]; the contact friction of non-vdW Fe_3O_4 is found much reduced at the 2D limit [28]; it is also noted that 2D α-Fe_2O_3 prefers the ferromagnetic ordering to the antiferromagnetic ordering which its bulk parent exhibits[29]; in addition, unlike vdW 2D materials for which the band gap generally increases down to monolayer, for non-layered oxide monolayers the structural reconstruction-induced band gap modulation is more material-specific and diverse.[23] Both band gap increase and decrease were observed in non-layered oxide monolayers.

Among non-layered oxides, TiO_2 has been intensively studied due to its multiple industrial applications.[30, 31] It is desirable to understand the structural reconstruction modulated physical properties of TiO_2 at the 2D limit so that the exploration of potential applications can be facilitated. In this study, based on a predicted stable monolayer TiO_2 structure, we report that its distinct structure at the 2D limit endows it with an intrinsic flat band at the valence band edge. We further reveal significant modulation in the electronic, polaronic and excitonic properties. The polaron state observed here turns out to provide a novel perspective to understand the aforementioned experimentally grown 2D TiO_2. The intrinsic flat band, the formation of small polarons, and the large excitonic binding energy in this TiO_2 monolayer shed light on understanding of diversified structural, optical and electronic properties of non-layered oxides at the monolayer limit.

Computational Method

The search for stable 2D TiO_2 structures was performed using the particle swarm optimization (PSO) method implemented in the CALYPSO program.[32, 33] This method has been widely used to predict novel 2D structures.[33-37] In the current PSO calculations, the stoichiometric formula of titanium oxide was constrained to TiO_2, and the number of formula units per simulation cell, the number of CALYPSO steps, and the number of configurations in each step were set to 16, 40, and 30, respectively.

The structural and electronic properties of the stable TiO_2 monolayers predicted by PSO were further studied by spin-polarized first-principles calculations using the Vienna ab initio simulation package (VASP.5.4.4.18)[38, 39] with the generalized gradient approximation (GGA) in the Perdew-Burke-Ernzerhof (PBE) form.[40] The interaction between valence electrons and ionic cores was approximated by the projector augmented-wave (PAW) method.[41] The electronic wave functions were expanded by a plane wave basis with a cutoff energy of 500

eV. Γ-centered *k*-point meshes of 9×9×1, 3×9×1, 6×6×1 and 3×3×1 were used to sample the first Brillouin zones of the TiO_2 2D unit cell (**Figure 1a**), and 3×1×1, 2×2×1, and 4×4×1 supercells, respectively. A vacuum layer of around 15 Å was inserted in the direction normal to the TiO_2 surface to minimize the spurious interaction between adjacent layers. The total energy and Hellmann-Feynman force on each atom were converged to 10^{-6} eV and 0.01 eV/Å, respectively. For structural relaxations, the GGA+*U* method was applied to the Ti 3*d* electrons with an effective *U* value of 4 eV.[42] The Heyd-Scuseria-Ernzerhof hybrid functional (HSE06) was used in the density of states and band structure calculations.[43] Investigations have shown that the HSE06 functional could accurately describe the electronic structure of both rutile and anatase TiO_2 bulks (HSE06/experimental band gap: 3.40/3.03 eV for rutile and 3.58/3.20 eV for anatase).[44, 45]

To simulate the polaron state, we introduced one excess electron in the TiO_2 2D unit cell and the 2×2×1 supercell and applied a small distortion to a selected Ti lattice site to break the lattice symmetry before the structural optimization using the GGA+*U* method (the *U* value varying in the range of 3.0-4.0 eV). This method has been widely adopted to model the polaron state in various oxide structures such as $FePO_4$, $BiVO_4$ and rutile-TiO_2.[46-50] We also consider the non-polaron state, in which the excess electron was introduced into the TiO_2 2D structure but without the initial perturbation. To simulate the interface between 2D TiO_2 and the rutile TiO_2 substrate, the Ti-terminated (011) surface of rutile TiO_2 was considered since the experimental growth of the aforementioned 2D TiO_2 was on the Ti-rich rutile TiO_2 (011) substrate.[17] The interface model was built by putting a $\sqrt{3} \times 1 \times 1$ supercell of 2D TiO_2 on top of the $2 \times 1 \times 1$ Ti-rich rutile TiO_2 substrate. Pseudo-hydrogen atoms were used to passivate the bottom oxygen of the substrate, which could mitigate the artificial impact of the bottom substrate termination on the concerned interface between supported 2D TiO_2 and the substrate.

The STM images were simulated using the Tersoff-Hamann model,[51] and visualized with a constant height of 1.5 Å above the TiO_2 surface. The optical spectrum was calculated using both the random phase approximation (RPA) and the Bethe-Salpeter equation (BSE) in the Tamm-Dancoff approximation[52] on top of the G_0W_0 results, in which the eight highest valence bands and the eight lowest conduction bands were chosen as the basis for excitonic eigenstates.

Results and Discussion

The atomic structure of monolayer TiO_2 considered here is shown in **Figure 1a**. This structure has been reported to be the ground state of 2D TiO_2,[45] which is further corroborated by our particle swarm optimization simulations. This 2D phase has a hexagonal lattice with the space group of P6/mmm and is referred to as hexagonal nanosheet (HNS). We are aware that various 2D TiO_2 structures have been predicted, where the relative stability might vary with the different exchange-correlation functionals used in the calculation.[45, 53] Nevertheless, the HNS TiO_2 structure has been found lower in energy than the experimentally synthesizable 2D anatase (ANS)-like phase regardless of chosen functionals (see **Table S1**).[21, 53] **Figure 1a** shows that the HNS TiO_2 contains 4 Ti and 8 O atoms per unit cell. The two AA stacked honeycomb Ti sublattices are connected by a honeycomb O sublattice in the middle. Each Ti sublattice is also interpenetrated by a surface Kagome O sublattice with the latter protruded. This establishes a double-layered corner-shared tetrahedron structure, similar to the reported silica bilayer structure.[12, 54, 55] It is noted that Ti atoms are octahedrally coordinated with O atoms in either anatase or rutile TiO_2 bulk instead of the tetrahedral coordination in 2D HNS TiO_2. This could be ascribed to the low atomic density of the latter (**Figure S1** in Supporting Information). The lattice constant of the optimized TiO_2 monolayer is $a = b = 6.125$ Å. There are two types of O atoms (denoted as O1 and O2 in **Figure 1a**). The Ti-O1 bond (1.84 Å) is slightly shorter than the Ti-O2 bond (1.86 Å). It is noted that the Ti-O bond length in this TiO_2 monolayer is at least 0.14 Å shorter than that of bulk rutile-TiO_2. A similar bond length

difference between 2D and bulk structures is also found in other 2D oxide structures.[15, 35] This can be ascribed to the reduced coordination and the suppression of surface polarization, which enhance the in-plane bonding in 2D oxides.

The electron localization function calculations show that the Ti-O bond in the monolayer TiO_2 is slightly more covalent-like compared with that in the rutile TiO_2 (**Figure S2**).[56] This is corroborated with the reduced Ti valence state based on the Bader charge analysis,[57] *i.e.*, $Ti^{+2.24}O_2^{-1.12}$ for monolayer TiO_2 and $Ti^{+2.36}O_2^{-1.18}$ for the rutile bulk. It is worth noting that the reduced Fe valence state of monolayer Fe_3O_4 has been identified as one of the key factors in stabilizing the structure.[28]

The reduced coordination and increased in-plane bonding strength in monolayer TiO_2 could lead to distinct electronic properties compared with its bulk counterparts. The electronic properties of the TiO_2 monolayer were investigated using the hybrid functional (HSE06) method. The projected density of states (PDOS) in **Figures 1b-c** show that the valence band edge states are mainly derived from the O atoms, while the Bloch states around the conduction band edge mostly arise from the Ti atoms. This indicates that it is a charge-transfer gap, analogous to that of rutile TiO_2.[58] It is noted that there are dense electronic states at around 3.0 eV below the Fermi level. As shown in **Figures 1c** and **S3**, they are dominated by the hybridization between the O1 p_x, p_y orbitals and the Ti $d_{xy}, d_{x^2-y^2}$ orbitals, and between the O2 p_z orbital and the Ti d_{z^2} orbital, which are favourable to stabilize oxide 2D structures.[59] Meanwhile, the hybridization between the O1 p_x, p_y orbitals and the Ti d_{xz}, d_{yz} orbitals is also noted due to the outward protrusion of the surface O1 sublattice (**Figures 1a** and **1c**). This unique electronic structure can be understood by analysing the distinct 2D O-Ti bonding network. Different from the three-fold coordinated O atoms in bulk anatase and rutile TiO_2, O atoms in the 2D structure are just bound to two neighbouring Ti atoms. According to the

electron counting model,[60] each O atom can get one electron from each O-Ti bond. Thus, the O *p* orbitals in the 2D TiO_2 structure will form a bonding paired state with neighbouring Ti *d* orbitals as well as two non-bonding paired states. As shown in **Figure 3S**, the bonding paired O2 p_z −Ti d_{z^2} state has a lower energy and a sharper peak near 3 eV below the Fermi level than the non-bonding O2 p_x, p_y paired states. For the O1 atom, due to the 6-fold rotational symmetry about the out-of-plane axis crossing the hexagonal center (**Figure 1a**), the hybridized O1 p_x and p_y orbitals will give rise to one bonding paired state with the neighbouring Ti *d* orbital along the Ti-O1 bond with lower energy and one non-bonding paired states with higher energy. These distinct non-bonding paired states near the Fermi level couple to the Kagome sublattice and likely lead to exotic properties, such as flat bands as elaborated below.[61]

Using the HSE06 hybrid functional, the band gap of the TiO_2 monolayer was calculated to be 4.8 eV with the valence band maximum (VBM) and the conduction band minimum (CBM) located at the Γ and K points, respectively (**Figure 2a**). At the G_0W_0 level of theory, the band gap further increases up to 6.0 eV (**Figure S4**). This band gap is about more than 2 eV larger than that of bulk TiO_2 (experimental band gap: 3.03 eV for rutile and 3.20 eV for anatase).[44, 45] On the other hand, the dimensionality reduction, the Kagome surface sublattices, and the lower atomic density also reduce the band dispersion of 2D TiO_2. In particular, a flat band can be seen at the valence band edge across the Brillouin zone, the bandwidth of which is 99 meV at the HSE06 level of theory. This flat band is mainly contributed by the surface Kagome O1 sublattices and slightly by the mid-layered O2 sublattice (see the PDOSs in **Figure S3**). The Kagome O1 sublattices also give rise to two Dirac bands which touch the flat band at the Γ point. A gap can be induced at the touching point by the spin-orbit coupling, suggesting this flat band to be topologically nontrivial.[61]

While there are two equivalent Kagome O1 sublattices, we noted that the flat band is not degenerate except at the Γ point. To understand the nondegeneracy and the minor dispersion

of the flat band, the tight-binding (TB) model was constructed. The Hamiltonian describing the interactions between oxygen sites can be written as:

$$\mathcal{H} = \sum_{\substack{i \\ \eta=\alpha,\beta,\gamma}} \varepsilon_{i\eta}^{0} c_{i\eta}^{\dagger} c_{i\eta} + \sum_{\substack{<i,j> \\ \eta=\alpha,\beta}} t_1 c_{i\eta}^{\dagger} c_{j\eta} + \sum_{<i,i>} t_2 c_{i\alpha}^{\dagger} c_{i\beta} + \sum_{\substack{<i,j> \\ \eta=\alpha,\beta}} t_3 c_{i\eta}^{\dagger} c_{j\gamma} + \sum_{<i,j>} t_4 c_{i\gamma}^{\dagger} c_{j\gamma} + \sum_{\substack{\ll i,j \gg \\ \eta=\alpha,\beta}} t_5 c_{i\eta}^{\dagger} c_{j\eta} + h.c.,$$

where $c_{i\eta}^{\dagger}$ ($c_{i\eta}$) is the creation (annihilation) operator for an electron on site i of oxygen sublattice η. α (β) denotes the top (bottom) surface O1 sublattice, and γ the middle-layer O2 sublattice. $\varepsilon_{i\eta}^{0}$ is the on-site energy of site i of sublattice η. $< i,j >$ ($\ll i,j \gg$) runs over all the nearest (next-nearest) neighbouring oxygen sites within oxygen sublattice η or between sublattices. $t_1 - t_5$ are the hopping amplitude between oxygen sites and are marked in **Figure 3**. When only the nearest neighbouring hoping within each surface Kagome O1 sublattice (t_1) is considered, a perfect double-degenerate Kagome band structure is produced (**Figure 3a**). By selectively turning on inter-site couplings, we can identify the one between the two surface Kagome O1 sublattices (t_2) which plays a key role in lifting the flat band degeneracy (see **Figure 3b**). This is in line with the predominant contribution from the O1 p_z orbital to the topmost valence band (**Figure S3**). There is also a noticeable interaction between O1 and O2 (t_3), which further modulates the dispersion of the Dirac bands of the Kagome O1 sublattices as well as the flat band associated with the O2 sublattice. The resulting TB bands are analogous to the DFT bands in **Figure 2a**, but the topmost flat band is still perfectly flat. The ~100 meV band width turns out to originate from the weak yet non-negligible coupling between next-nearest neighbouring O1 atoms within each surface Kagome sublattice (t_5), as shown in **Figure 3e**.

The topologically nontrivial intrinsic flat band in the TiO_2 monolayer may host exotic many-body quantum phenomena, such as Mott transition,[62] Wigner crystallization,[63, 64] superconductivity,[65] fractional quantum anomalous Hall effect[66, 67], and large exciton binding energy.[68] One notes that the minor valence band dispersion suggests a very large effective mass of hole (m_h) in the TiO_2 monolayer. According to $\mu = \frac{m_e m_h}{m_e + m_h}$ (m_e: the effective mass of electron), the effective mass of exciton would be large as well. As such, a large exciton binding energy can be expected in the TiO_2 monolayer.[69, 70] Here, our calculations estimate the exciton binding energy to be ~2.49 eV in this TiO_2 monolayer (**Figure 2b**). It is much larger than that in the anatase TiO_2 bulk (~1.0 eV),[71] implying a much stronger light-matter interaction. In

addition, the porous structure and atomically thin thickness further weaken the screening effect and thus contribute to the large exciton binding energy as well. The weak screening effect in the monolayer limit also suggests strong coupling between charge and lattice, as discussed in the following.

Polarons are a type of quasiparticle composed of a charge carrier and its self-induced virtual phonon cloud. The polaron state forms when a charge carrier strongly interacts with the host lattice and is trapped around one or a few lattice sites, whereas the non-polaron state corresponds to a weak interaction with the lattice and a nearly homogenous distribution of the charge carrier. TiO_2 is one of the historically most studied polaron materials.[72] Excess electrons migrating in rutile TiO_2 have been found to strongly interact with the Ti lattice and form small polarons, while the anatase phase is prone to the formation of large electron polarons.[47, 73] The different polaron behaviours of rutile and anatase TiO_2 affect their respective intrinsic properties as well as technological applications.[47] Herein, the polaron behaviour in the monolayer TiO_2 was further investigated. For metal oxides, the standard DFT solutions are usually more delocalized than they should be due to the presence of the self-interaction error. Both the DFT+*U* method and the hybrid functionals have been widely adopted to alleviate this error.[72] In this study, we adopted the former method and chose the well-studied rutile TiO_2 as a reference system. The propensity to small polaron formations can be evaluated by the minimum Hubbard *U* value which is required to stabilise the polaron state over the non-polaron state, *i.e.*, the free-carrier state.[47] The smaller the required Hubbard *U* value is, the more likely are small polarons to form. **Figure 4a** summarizes the dependence of the relative stability of the polaron state on the Hubbard *U* value. One sees that the monolayer TiO_2 (the 2×2×1 supercell) needs a similar minimum *U* value to energetically stabilise the polaron state compared with rutile TiO_2 (the 3×3×4 supercell), indicating the high likelihood that electrons would be trapped by their self-induced potential well. At the Hubbard *U* value of 4 eV, the polaron state is 227 meV lower in energy than the non-polaron state. This could be ascribed to the narrow conduction band of monolayer TiO_2 (**Figure S5**).[47] The lower coordination of the Ti site (4 in the 2D structure and 6 in the rutile structure) and the higher structural flexibility may also contribute to the stabilization of the polaron state in the monolayer TiO_2.[50]

Note that the HSE06 functional has been reported to well describe the electronic structure of both rutile and anatase TiO_2 bulks (HSE06/experimental band gap: 3.40/3.03 eV for rutile and 3.58/3.20 eV for anatase).[44, 45] Here we switched to the HSE06 functional to calculate the PDOSs of the polaron state in monolayer TiO_2, as shown in **Figures 4b** and **S6**. When an excess

electron is available in the monolayer TiO_2, it mainly fills the lowest Ti $d_{x^2-y^2}$ and d_{xz} states of the conduction band. To lower the system energy, these filled states split from the unoccupied Ti states, shift towards lower energy and form a narrow mid-gap state. It is at ~1 eV below the conduction band edge, which is on the typical energy splitting scale of small polarons.[72] The partial charge associated with this mid-gap state in **Figure 4c** shows that the excess electron in the polaron state is mostly localized on a Ti site, in stark contrast with the homogeneous distribution across the whole Ti sublattice (**Figure S7**) in the non-polaron state. The trapped electron density is tilted in such a way that it extends towards voids around the Ti site, rather than the neighbouring O sites. The half-maximum width is estimated within 1.5 Å, which is around one quarter of the lattice constant of the TiO_2 monolayer (**Figure 4d**). Apart from the electronic structure reconstruction, pronounced local lattice distortions around the Ti site are also observed. In order to accommodate the excess electron, the Ti atom exhibits weaker chemical bonding with its neighbouring oxygen atoms, as evidenced by the 0.08−0.13 Å Ti-O bond length elongation relative to the non-polaron state (**Table S2**). It is also noted that such local bond length variation induced by the polaron formation is more significant in monolayer TiO_2 than in the rutile-phase TiO_2 (see **Table S2**). All these characteristics suggest that the polaron formed in the monolayer belongs to the small polaron. The preference to the formation of small polarons may suggest 2D TiO_2 as a potential photocatalyst. On the one hand, the filled mid-gap state significantly reduces the band gap and substantially extend its solar energy conversion capability to the visible light regime. One the other hand, the 2D nature exposes most small polarons, which could facilitate the charge transfer to adsorbates or modulate their adsorption behaviour in catalytic processes.[47, 74]

As mentioned above, the formation of small polarons in 2D TiO_2 can greatly reduce its band gap due to the presence of the mid-gap state. The extent to which the electronic structure is altered is in fact dependent on the charge carrier density. Interestingly, we found that the formation of small polarons in combination with the substrate effects could provide a new perspective to understand the monolayer TiO_2 grown on the rutile TiO_2 (011) surface.[17] The widely observed substrate effects include the interface charge transfer and the strain effect due to the lattice mismatch. Since the rutile TiO_2 (011) substrate is slightly reduced and rich in Ti,[17] electrons could be transferred from the substrate to the TiO_2 monolayer, as evidenced by the considerable charge redistribution at the interface (**Figure 5a**). The dramatic difference in the lattice symmetry and periodicity between the substrate and the as-synthesized monolayer implies that the latter is somewhat strained. When both substrate effects are taken into account

by introducing an excess electron and applying a compressive strain of ~6.3 %, it is striking that the formation of small polarons could reduce the band gap of the 2D TiO_2 structure proposed here to 2.2 eV at the HSE06 level of theory. It is very close to the experimental value of ~2.1 eV.[17] In the meantime, the distinct lattice pattern of the as-synthesized TiO_2 monolayer can also be well reproduced by our STM simulation of the small polaron state (see **Figure 5c**).

Conclusions

In conclusion, we unravel the structural reconstruction modulated electronic, polaronic and excitonic properties of a stable monolayer TiO_2 using first-principles calculations and tight-binding model. We find that the monolayer TiO_2 has a large band gap and its surface Kagome oxygen sublattices could induce a topologically nontrivial intrinsic flat band near the valence band edge. Such a flat band gives rise to an unprecedentedly large exciton binding energy. We further show that the monolayer TiO_2 favors the formation of small polarons, which significantly reduces the band gap to the visible light range, indicative of its potential application in photovoltaics and photocatalysis. In addition, in combination of the substrate effects and the small polaron state, the simulated surface lattice, the reduced band gap, and the simulated STM image in the monolayer TiO_2 are consistent with those of the experimentally observed 2D TiO_2 phase.[17] These findings not only highlight the dimensionality reduction-induced modulation of various intrinsic properties for non-layered materials, but also shed light on understanding of the experimentally grown TiO_2 2D phase. In addition, the intrinsic flat band in the non-layered 2D oxide monolayer might suggest them to be a promising platform to investigate the strong correlation effect and its induced exotic quantum phenomena.

Supporting Information

The Supporting Information is available free of charge at https://pubs.acs.org/doi/xxx.

Coordination environment analysis; Bonding information; (Projected) density of states and electronic band structures of pristine and polaron-state TiO_2; Visualization of polaron and non-polaron states of TiO_2; Relative stability of 2D TiO_2 phases.

Acknowledgements

M.Y. acknowledges the funding support from The Hong Kong Polytechnic University (project number: 1-BE47, ZE0C, ZE2F and ZE2X) and State Key Laboratory of Advanced Technology for Float Glass, China (project number: 2010DQ710341). T.Y. would like to acknowledge Singapore MOE Tier 2 grant (MOE2019-T2-2-30). We acknowledge Centre for Advanced 2D Materials, Centre of Information Technology at National University of Singapore, and the National Supercomputing Centre Singapore for providing computing resources.

References

(1) Novoselov, K. S.; Geim, A. K.; Morozov, S. V.; Jiang, D.; Zhang, Y.; Dubonos, S. V.; Grigorieva, I. V.; Firsov, A. A. Electric Field Effect in Atomically Thin Carbon Films. *Science* **2004**, *306* (5696), 666-669

(2) Xu, M.; Liang, T.; Shi, M.; Chen, H. Graphene-Like Two-Dimensional Materials. *Chem. Rev.* **2013**, *113* (5), 3766-3798

(3) Roy, T.; Tosun, M.; Kang, J. S.; Sachid, A. B.; Desai, S. B.; Hettick, M.; Hu, C. C.; Javey, A. Field-Effect Transistors Built from All Two-Dimensional Material Components. *ACS Nano* **2014**, *8* (6), 6259-6264

(4) Miró, P.; Audiffred, M.; Heine, T. An atlas of two-dimensional materials. *Chem. Soc. Rev.* **2014**, *43* (18), 6537-6554

(5) Kubota, Y.; Watanabe, K.; Tsuda, O.; Taniguchi, T. Deep Ultraviolet Light-Emitting Hexagonal Boron Nitride Synthesized at Atmospheric Pressure. *Science* **2007**, *317* (5840), 932-934

(6) Mak, K. F.; Lee, C.; Hone, J.; Shan, J.; Heinz, T. F. Atomically Thin MoS_2: A New Direct-Gap Semiconductor. *Phys. Rev. Lett.* **2010**, *105* (13), 136805

(7) Kuc, A.; Zibouche, N.; Heine, T. Influence of quantum confinement on the electronic structure of the transition metal sulfide TS_2. *Phys. Rev. B* **2011**, *83* (24), 245213

(8) Zhuang, H. L.; Hennig, R. G. Single-Layer Group-III Monochalcogenide Photocatalysts for Water Splitting. *Chem. Mater.* **2013**, *25* (15), 3232-3238

(9) Zheng, J.; Zhang, H.; Dong, S.; Liu, Y.; Tai Nai, C.; Suk Shin, H.; Young Jeong, H.; Liu, B.; Ping Loh, K. High yield exfoliation of two-dimensional chalcogenides using sodium naphthalenide. *Nat. Commun.* **2014**, *5* (1), 2995

(10) Cunningham, G.; Lotya, M.; Cucinotta, C. S.; Sanvito, S.; Bergin, S. D.; Menzel, R.; Shaffer, M. S. P.; Coleman, J. N. Solvent Exfoliation of Transition Metal Dichalcogenides: Dispersibility of Exfoliated Nanosheets Varies Only Weakly between Compounds. *ACS Nano* **2012**, *6* (4), 3468-3480

(11) Li, L.; Yu, Y.; Ye, G. J.; Ge, Q.; Ou, X.; Wu, H.; Feng, D.; Chen, X. H.; Zhang, Y. Black phosphorus field-effect transistors. *Nat. Nanotechnol.* **2014**, *9* (5), 372-377

(12) Löffler, D.; Uhlrich, J. J.; Baron, M.; Yang, B.; Yu, X.; Lichtenstein, L.; Heinke, L.; Büchner, C.; Heyde, M.; Shaikhutdinov, S.; et al. Growth and Structure of Crystalline Silica Sheet on Ru(0001). *Phys. Rev. Lett.* **2010**, *105* (14), 146104

(13) Zavabeti, A.; Ou, J. Z.; Carey, B. J.; Syed, N.; Orrell-Trigg, R.; Mayes, E. L. H.; Xu, C.; Kavehei, O.; O'Mullane, A. P.; Kaner, R. B.; et al. A liquid metal reaction environment for the room-temperature synthesis of atomically thin metal oxides. *Science* **2017**, *358* (6361), 332-335

(14) Zhang, B. Y.; Xu, K.; Yao, Q.; Jannat, A.; Ren, G.; Field, M. R.; Wen, X.; Zhou, C.; Zavabeti, A.; Ou, J. Z. Hexagonal metal oxide monolayers derived from the metal–gas interface. *Nat. Mater.* **2021**, *20* (8), 1073-1078

(15) Song, T. T.; Yang, M.; Callsen, M.; Wu, Q. Y.; Zhou, J.; Wang, S. F.; Wang, S. J.; Feng, Y. P. Graphene stabilized high-κ dielectric Y_2O_3(111) monolayers and their interfacial properties. *RSC Adv.* **2015**, *5* (102), 83588-83593

(16) Yang, T.; Song, T. T.; Callsen, M.; Zhou, J.; Chai, J. W.; Feng, Y. P.; Wang, S. J.; Yang, M. Atomically Thin 2D Transition Metal Oxides: Structural Reconstruction, Interaction with Substrates, and Potential Applications. *Adv. Mater. Interfaces* **2019**, *6* (1), 1801160

(17) Tao, J.; Luttrell, T.; Batzill, M. A two-dimensional phase of TiO_2 with a reduced bandgap. *Nat. Chem.* **2011**, *3* (4), 296-300

(18) Yang, J.-H.; Zhang, Y.; Yin, W.-J.; Gong, X. G.; Yakobson, B. I.; Wei, S.-H. Two-Dimensional SiS Layers with Promising Electronic and Optoelectronic Properties: Theoretical Prediction. *Nano Lett.* **2016**, *16* (2), 1110-1117

(19) Addou, R.; Dahal, A.; Batzill, M. Growth of a two-dimensional dielectric monolayer on quasi-freestanding graphene. *Nat. Nanotechnol.* **2013**, *8* (1), 41-45

(20) Matsuzaki, K.; Hosono, H.; Susaki, T. Layer-by-layer epitaxial growth of polar MgO(111) thin films. *Phys. Rev. B* **2010**, *82* (3), 033408

(21) Sun, Z.; Liao, T.; Dou, Y.; Hwang, S. M.; Park, M.-S.; Jiang, L.; Kim, J. H.; Dou, S. X. Generalized self-assembly of scalable two-dimensional transition metal oxide nanosheets. *Nat. Commun.* **2014**, *5* (1), 3813

(22) Lu, Y. H.; Xu, B.; Zhang, A. H.; Yang, M.; Feng, Y. P. Hexagonal TiO_2 for Photoelectrochemical Applications. *J. Phys. Chem. C* **2011**, *115* (36), 18042-18045

(23) sFriedrich, R.; Ghorbani-Asl, M.; Curtarolo, S.; Krasheninnikov, A. V. Data-Driven Quest for Two-Dimensional Non-van der Waals Materials. *Nano Lett.* **2022**, *22* (3), 989-997

(24) Wang, Q.; Oganov, A. R.; Feya, O. D.; Zhu, Q.; Ma, D. The unexpectedly rich reconstructions of rutile TiO_2(011)-(2×1) surface and the driving forces behind their formation: an ab initio evolutionary study. *Phys. Chem. Chem. Phys.* **2016**, *18* (29), 19549-19556

(25) Zhou, R.; Li, D.; Qu, B.; Sun, X.; Zhang, B.; Zeng, X. C. Rutile TiO_2(011)-2×1 Reconstructed Surfaces with Optical Absorption over the Visible Light Spectrum. *ACS Appl. Mater. Interfaces* **2016**, *8* (40), 27403-27410

(26) Xu, M.; Shao, S.; Gao, B.; Lv, J.; Li, Q.; Wang, Y.; Wang, H.; Zhang, L.; Ma, Y. Anatase (101)-like Structural Model Revealed for Metastable Rutile TiO_2(011) Surface. *ACS Appl. Mater. Interfaces* **2017**, *9* (9), 7891-7896

(27) Wilk, G. D.; Wallace, R. M.; Anthony, J. M. High-κ gate dielectrics: Current status and materials properties considerations. *J. Appl. Phys.* **2001**, *89* (10), 5243-5275

(28) Serles, P.; Arif, T.; Puthirath, A. B.; Yadav, S.; Wang, G.; Cui, T.; Balan, A. P.; Yadav, T. P.; Thibeorchews, P.; Chakingal, N.; et al. Friction of magnetene, a non-van der Waals 2D material. *Sci. Adv.* **2021**, *7* (47), eabk2041

(29) Puthirath Balan, A.; Radhakrishnan, S.; Woellner, C. F.; Sinha, S. K.; Deng, L.; Reyes, C. d. l.; Rao, B. M.; Paulose, M.; Neupane, R.; Apte, A.; et al. Exfoliation of a non-van der Waals material from iron ore hematite. *Nat. Nanotechnol.* **2018**, *13* (7), 602-609

(30) Haider, A. J.; Jameel, Z. N.; Al-Hussaini, I. H. M. Review on: Titanium Dioxide Applications. *Energy Procedia* **2019**, *157*, 17-29

(31) Chen, X.; Mao, S. S. Titanium Dioxide Nanomaterials: Synthesis, Properties, Modifications, and Applications. *Chem. Rev.* **2007**, *107* (7), 2891-2959

(32) Wang, Y.; Lv, J.; Zhu, L.; Ma, Y. CALYPSO: A method for crystal structure prediction. *Comput. Phys. Commun.* **2012**, *183* (10), 2063-2070

(33) Wang, Y.; Miao, M.; Lv, J.; Zhu, L.; Yin, K.; Liu, H.; Ma, Y. An effective structure prediction method for layered materials based on 2D particle swarm optimization algorithm. *J. Chem. Phys.* **2012**, *137* (22), 224108

(34) Yang, L.-M.; Bačić, V.; Popov, I. A.; Boldyrev, A. I.; Heine, T.; Frauenheim, T.; Ganz, E. Two-Dimensional Cu_2Si Monolayer with Planar Hexacoordinate Copper and Silicon Bonding. *J. Am. Chem. Soc.* **2015**, *137* (7), 2757-2762

(35) Song, T. T.; Yang, M.; Chai, J. W.; Callsen, M.; Zhou, J.; Yang, T.; Zhang, Z.; Pan, J. S.; Chi, D. Z.; Feng, Y. P.; et al. The stability of aluminium oxide monolayer and its interface with two-dimensional materials. *Sci. Rep.* **2016**, *6* (1), 29221

(36) Yang, T.; Luo, Y. Z.; Wang, Z.; Zhu, T.; Pan, H.; Wang, S.; Lau, S. P.; Feng, Y. P.; Yang, M. Ag_2S monolayer: an ultrasoft inorganic Lieb lattice. *Nanoscale* **2021**, *13* (33), 14008-14015

(37) Feng, B.; Fu, B.; Kasamatsu, S.; Ito, S.; Cheng, P.; Liu, C.-C.; Feng, Y.; Wu, S.; Mahatha, S. K.; Sheverdyaeva, P.; et al. Experimental realization of two-dimensional Dirac nodal line fermions in monolayer Cu_2Si. *Nat. Commun.* **2017**, *8* (1), 1007

(38) Kresse, G.; Hafner, J. Ab initio molecular dynamics for open-shell transition metals. *Phys. Rev. B* **1993**, *48* (17), 13115-13118
(39) Kresse, G.; Hafner, J. Ab initio molecular dynamics for liquid metals. *Phys. Rev. B* **1993**, *47* (1), 558-561
(40) Perdew, J. P.; Burke, K.; Ernzerhof, M. Generalized Gradient Approximation Made Simple. *Phys. Rev. Lett.* **1996**, *77* (18), 3865-3868
(41) Blöchl, P. E. Projector augmented-wave method. *Phys. Rev. B* **1994**, *50* (24), 17953-17979
(42) Dudarev, S. L.; Botton, G. A.; Savrasov, S. Y.; Humphreys, C. J.; Sutton, A. P. Electron-energy-loss spectra and the structural stability of nickel oxide: An LSDA+U study. *Phys. Rev. B* **1998**, *57* (3), 1505-1509
(43) Heyd, J.; Scuseria, G. E.; Ernzerhof, M. Hybrid functionals based on a screened Coulomb potential. *J. Chem. Phys.* **2003**, *118* (18), 8207-8215
(44) Scanlon, D. O.; Dunnill, C. W.; Buckeridge, J.; Shevlin, S. A.; Logsdail, A. J.; Woodley, S. M.; Catlow, C. R. A.; Powell, M. J.; Palgrave, R. G.; Parkin, I. P.; et al. Band alignment of rutile and anatase TiO_2. *Nat. Mater.* **2013**, *12* (9), 798-801
(45) Eivari, H. A.; Ghasemi, S. A.; Tahmasbi, H.; Rostami, S.; Faraji, S.; Rasoulkhani, R.; Goedecker, S.; Amsler, M. Two-Dimensional Hexagonal Sheet of TiO_2. *Chem. Mater.* **2017**, *29* (20), 8594-8603
(46) Chrétien, S.; Metiu, H. Electronic Structure of Partially Reduced Rutile TiO_2(110) Surface: Where Are the Unpaired Electrons Located? *J. Phys. Chem. C* **2011**, *115* (11), 4696-4705
(47) Setvin, M.; Franchini, C.; Hao, X.; Schmid, M.; Janotti, A.; Kaltak, M.; Van de Walle, C. G.; Kresse, G.; Diebold, U. Direct View at Excess Electrons in TiO_2 Rutile and Anatase. *Phys. Rev. Lett.* **2014**, *113* (8), 086402
(48) Chaudhuri, A.; Mandal, L.; Chi, X.; Yang, M.; Scott, M. C.; Motapothula, M.; Yu, X. J.; Yang, P.; Shao-Horn, Y.; Venkatesan, T.; et al. Direct observation of anisotropic small-hole polarons in an orthorhombic structure of $BiVO_4$ films. *Phys. Rev. B* **2018**, *97* (19), 195150
(49) Wang, Z.; Bevan, K. H. Exploring the impact of semicore level electronic relaxation on polaron dynamics: An adiabatic ab initio study of $FePO_4$. *Phys. Rev. B* **2016**, *93* (2), 024303
(50) Kong, W.; Zhou, J.; Luo, Y. Z.; Yang, T.; Wang, S.; Chen, J.; Rusydi, A.; Feng, Y. P.; Yang, M. Formation of two-dimensional small polarons at the conducting $LaAlO_3/SrTiO_3$ interface. *Phys. Rev. B* **2019**, *100* (8), 085413
(51) Tersoff, J.; Hamann, D. R. Theory and Application for the Scanning Tunneling Microscope. *Phys. Rev. Lett.* **1983**, *50* (25), 1998-2001

(52) Paier, J.; Marsman, M.; Kresse, G. Dielectric properties and excitons for extended systems from hybrid functionals. *Phys. Rev. B* **2008**, *78* (12), 121201

(53) Kim, I.; Lee, G.; Choi, M. First-principles investigation of two-dimensional 1T-TiO_2. *Phys. Rev. Mater.* **2020**, *4* (9), 094001

(54) Yang, B.; Kaden, W. E.; Yu, X.; Boscoboinik, J. A.; Martynova, Y.; Lichtenstein, L.; Heyde, M.; Sterrer, M.; Włodarczyk, R.; Sierka, M.; et al. Thin silica films on Ru(0001): monolayer, bilayer and three-dimensional networks of [SiO_4] tetrahedra. *Phys. Chem. Chem. Phys.* **2012**, *14* (32), 11344-11351

(55) Özçelik, V. O.; Cahangirov, S.; Ciraci, S. Stable Single-Layer Honeycomblike Structure of Silica. *Phys. Rev. Lett.* **2014**, *112* (24), 246803

(56) Becke, A. D.; Edgecombe, K. E. A simple measure of electron localization in atomic and molecular systems. *J. Chem. Phys.* **1990**, *92* (9), 5397-5403

(57) Henkelman, G.; Arnaldsson, A.; Jónsson, H. A fast and robust algorithm for Bader decomposition of charge density. *Comput. Mater. Sci.* **2006**, *36* (3), 354-360

(58) Cho, E.; Han, S.; Ahn, H.-S.; Lee, K.-R.; Kim, S. K.; Hwang, C. S. First-principles study of point defects in rutile TiO_{2-x}. *Phys. Rev. B* **2006**, *73* (19), 193202

(59) Zhuang, H. L.; Singh, A. K.; Hennig, R. G. Computational discovery of single-layer III-V materials. *Phys. Rev. B* **2013**, *87* (16), 165415

(60) Pashley, M. D. Electron counting model and its application to island structures on molecular-beam epitaxy grown GaAs(001) and ZnSe(001). *Phys. Rev. B* **1989**, *40* (15), 10481-10487

(61) Liu, H.; Meng, S.; Liu, F. Screening two-dimensional materials with topological flat bands. *Phys. Rev. Mater.* **2021**, *5* (8), 084203

(62) Cao, Y.; Fatemi, V.; Fang, S.; Watanabe, K.; Taniguchi, T.; Kaxiras, E.; Jarillo-Herrero, P. Unconventional superconductivity in magic-angle graphene superlattices. *Nature* **2018**, *556* (7699), 43-50

(63) Wu, C.; Bergman, D.; Balents, L.; Das Sarma, S. Flat Bands and Wigner Crystallization in the Honeycomb Optical Lattice. *Phys. Rev. Lett.* **2007**, *99* (7), 070401

(64) Jaworowski, B.; Güçlü, A. D.; Kaczmarkiewicz, P.; Kupczyński, M.; Potasz, P.; Wójs, A. Wigner crystallization in topological flat bands. *New J. Phys.* **2018**, *20* (6), 063023

(65) Miyahara, S.; Kusuta, S.; Furukawa, N. BCS theory on a flat band lattice. *Phys. C: Supercond.* **2007**, *460-462*, 1145-1146

(66) Tang, E.; Mei, J.-W.; Wen, X.-G. High-Temperature Fractional Quantum Hall States. *Phys. Rev. Lett.* **2011**, *106* (23), 236802

(67) Neupert, T.; Santos, L.; Chamon, C.; Mudry, C. Fractional Quantum Hall States at Zero Magnetic Field. *Phys. Rev. Lett.* **2011**, *106* (23), 236804
(68) Sethi, G.; Zhou, Y.; Zhu, L.; Yang, L.; Liu, F. Flat-Band-Enabled Triplet Excitonic Insulator in a Diatomic Kagome Lattice. *Phys. Rev. Lett.* **2021**, *126* (19), 196403
(69) Fogler, M. M.; Butov, L. V.; Novoselov, K. S. High-temperature superfluidity with indirect excitons in van der Waals heterostructures. *Nat. Commun.* **2014**, *5* (1), 4555
(70) Jiang, Z.; Liu, Z.; Li, Y.; Duan, W. Scaling Universality between Band Gap and Exciton Binding Energy of Two-Dimensional Semiconductors. *Phys. Rev. Lett.* **2017**, *118* (26), 266401
(71) Baldini, E.; Chiodo, L.; Dominguez, A.; Palummo, M.; Moser, S.; Yazdi-Rizi, M.; Auböck, G.; Mallett, B. P. P.; Berger, H.; Magrez, A.; et al. Strongly bound excitons in anatase TiO_2 single crystals and nanoparticles. *Nat. Commun.* **2017**, *8* (1), 13
(72) Franchini, C.; Reticcioli, M.; Setvin, M.; Diebold, U. Polarons in materials. *Nat. Rev. Mater.* **2021**, *6* (7), 560-586
(73) Verdi, C.; Caruso, F.; Giustino, F. Origin of the crossover from polarons to Fermi liquids in transition metal oxides. *Nat. Commun.* **2017**, *8* (1), 15769
(74) Reticcioli, M.; Sokolović, I.; Schmid, M.; Diebold, U.; Setvin, M.; Franchini, C. Interplay between Adsorbates and Polarons: CO on Rutile TiO_2 (110). *Phys. Rev. Lett.* **2019**, *122* (1), 016805

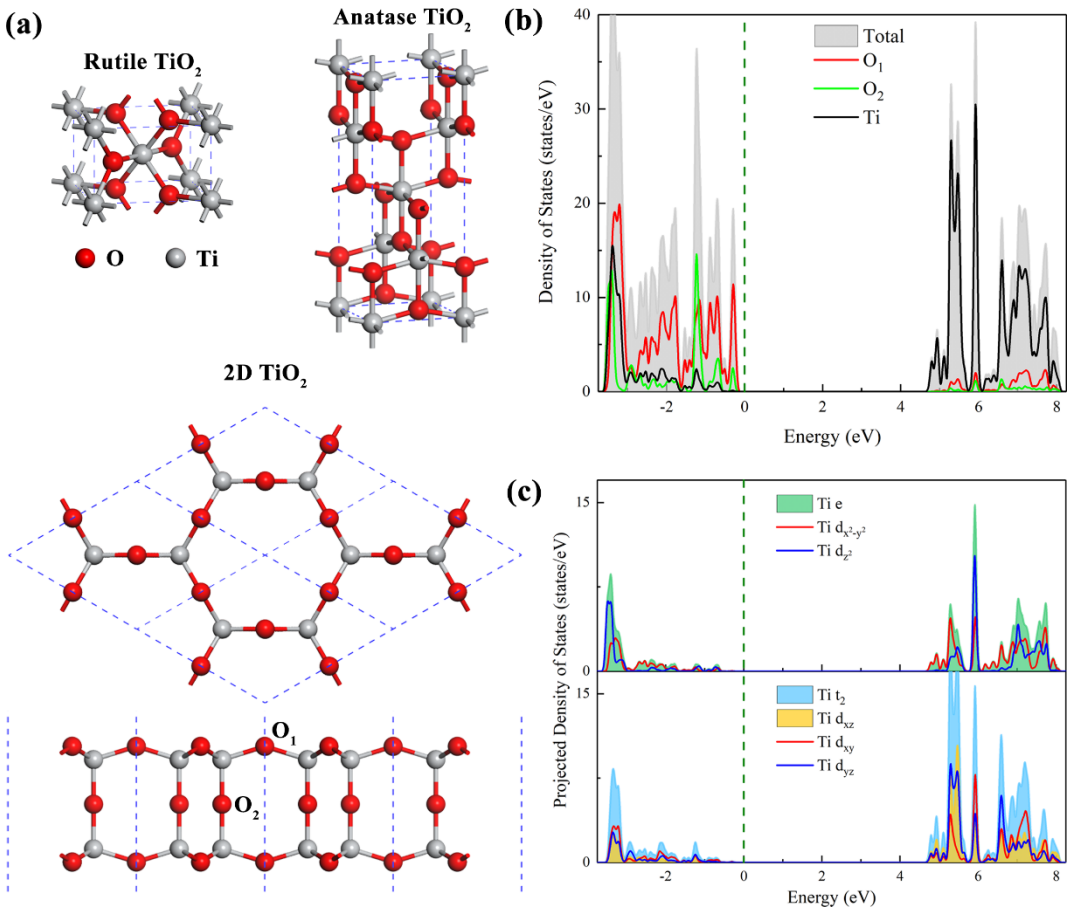

Figure 1. (a) The atomic structure of rutile, anatase and 2D TiO_2. (b-c) The projected density of states onto (b) Ti and O atoms, and (c) Ti *d* orbitals of the TiO_2 2D structure at the HSE06 level of theory. The Fermi level is shifted to 0 eV.

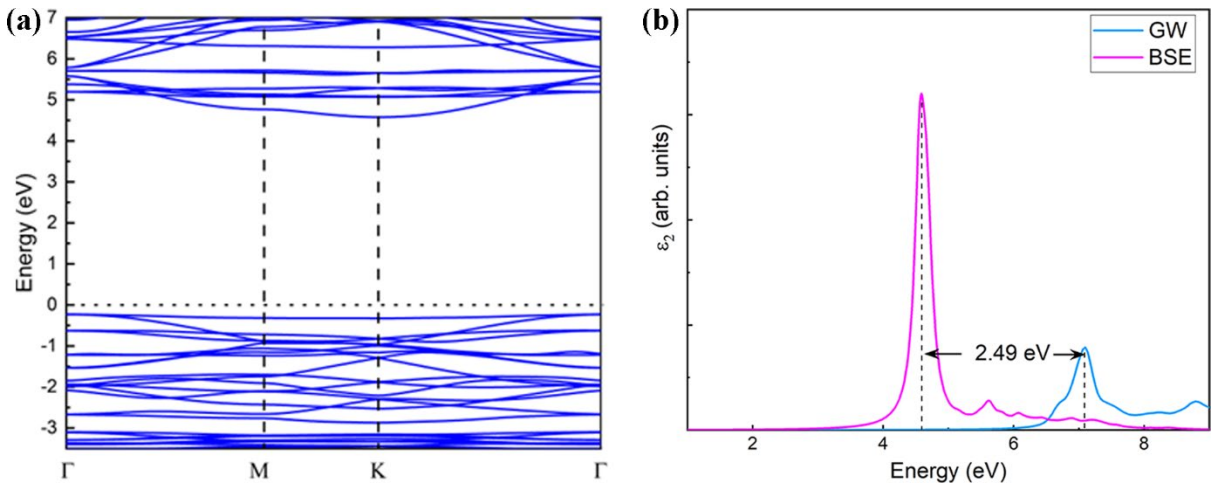

Figure 2. (a) The HSE06 band structure and (b) the optical spectra of the TiO_2 2D structure, respectively.

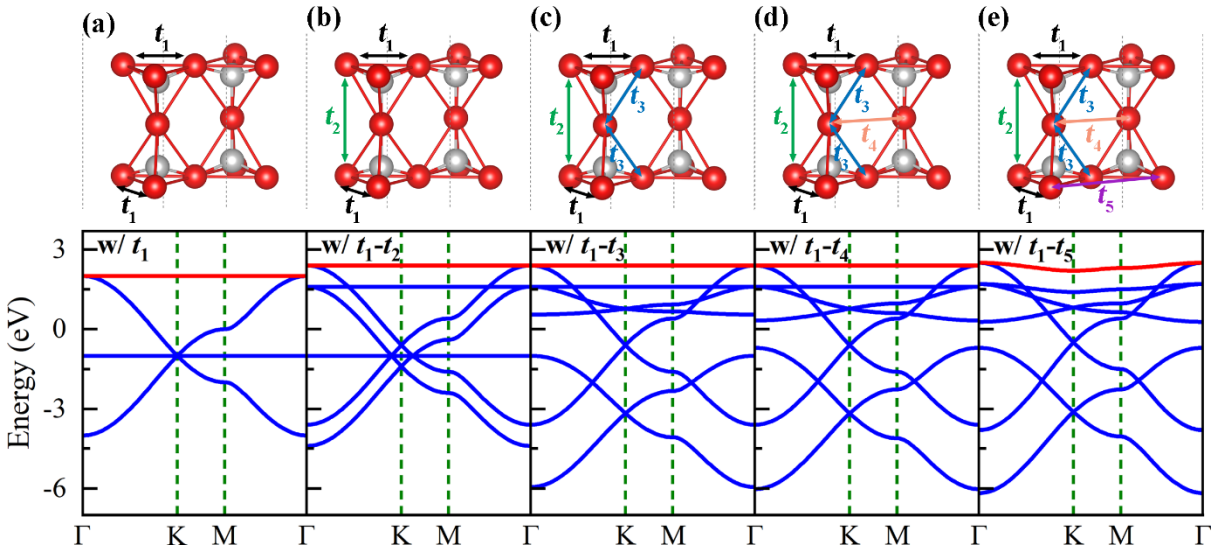

Figure 3. (a-e) The tight-binding model of 2D TiO_2 with the hoping between neighbouring oxygen atoms progressively considered. The upper panel marks the considered inter-site hoping and the bottom panel is the corresponding TB band structure. The hoping parameters are set to $t_1 = -1$, $t_2 = -0.4$, $t_3 = -0.8$, $t_4 = -0.1$ and $t_5 = -0.05$ eV. The on-site energies are set to $\varepsilon_{i\alpha}^0 = \varepsilon_{i\beta}^0 = 0$ eV and $\varepsilon_{i\gamma}^0 = -1$ eV.

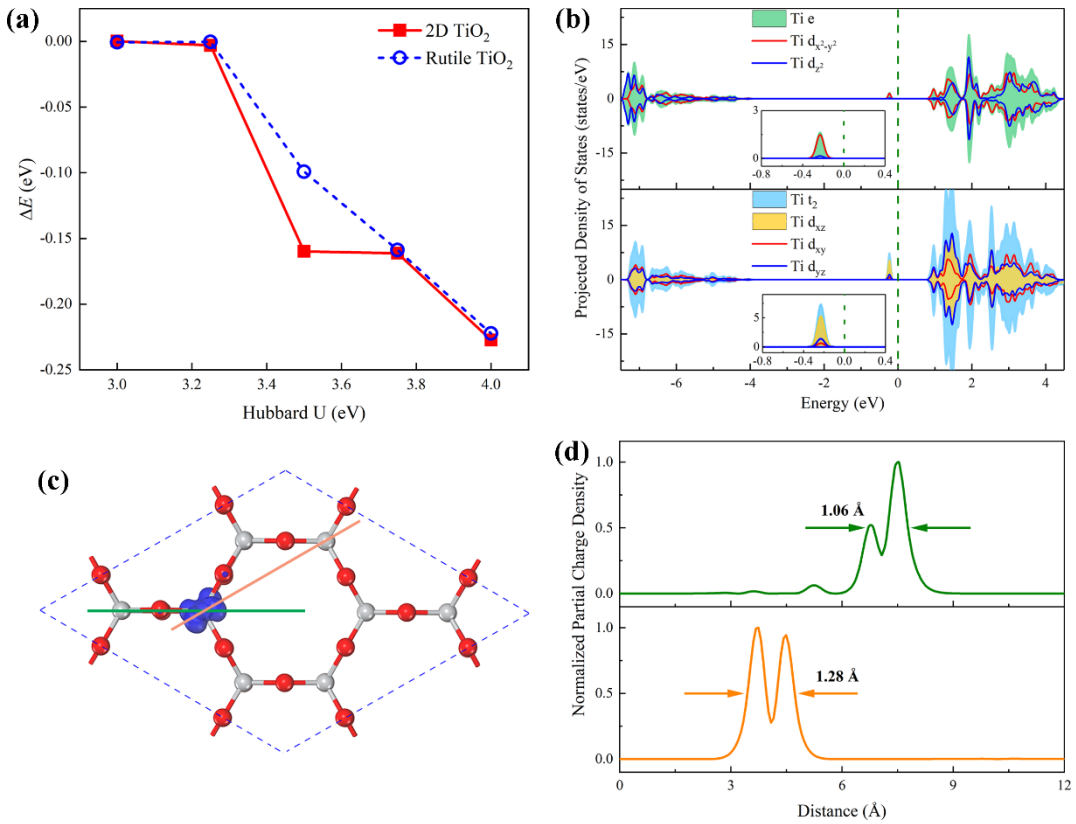

Figure 4. (a) The stability of the polaron state relative to the non-polaron state in the 2×2×1 2D and 3×3×4 rutile TiO_2 structure as a function of the Hubbard *U* value. (b) The projected density of states onto the Ti orbitals of the polaron state in the 2×2×1 2D TiO_2 at the HSE06 level of theory. The Fermi level is shifted to 0 eV. (c) The visualized partial charge density (top view) and (d) its line profiles of the mid-gap state in (b). The iso-value is set to 1.0×10^{-3} e/Å^3. The line profiles are along the lines marked in (c) at the height of the top O_1 atoms.

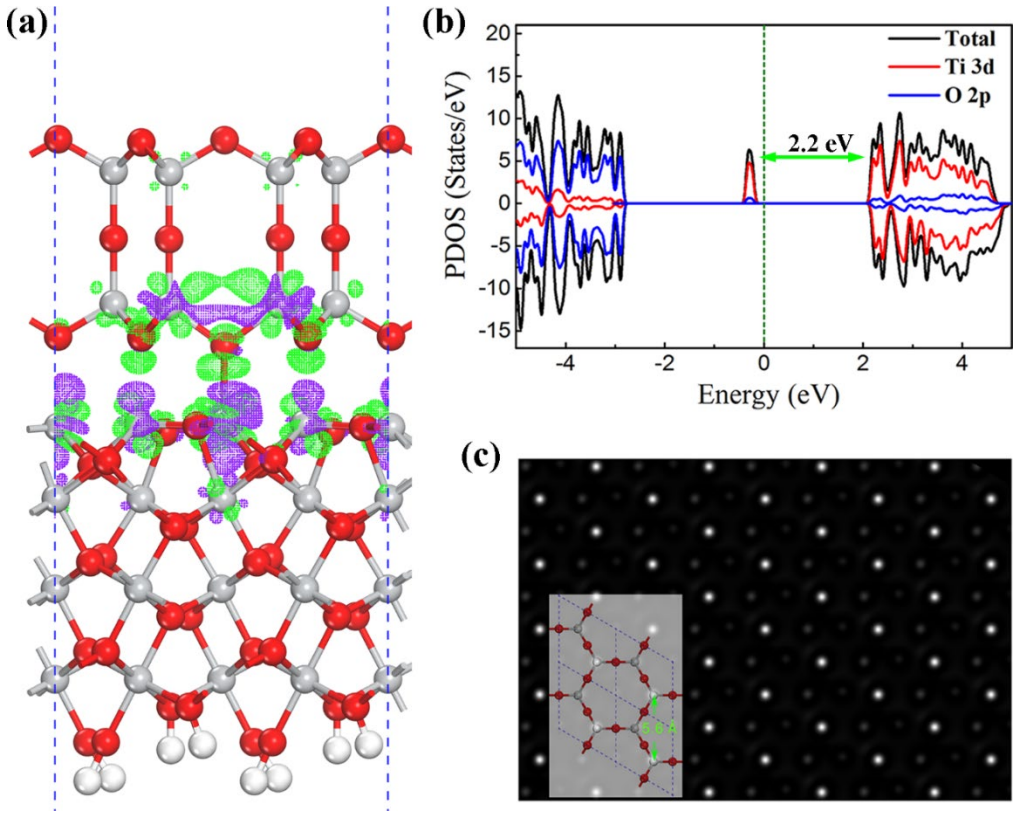

Figure 5. (a) The side view of the atomic structure for the TiO_2 2D structure on the rutile-TiO_2 (011) substrate superimposed with the charge density difference using an iso-value of 1.0×10^{-3} e/Å^3. The green and purple dots denote the accumulated and depleted charge, respectively. (b) The PDOSs of the 6.3% compressed TiO_2 2D unit cell structure in the small polaron state at the HSE06 level of theory. (c) The simulated STM image associated with the mid-gap state in (b), where the atomic structure is superimposed.

TOC Graphic

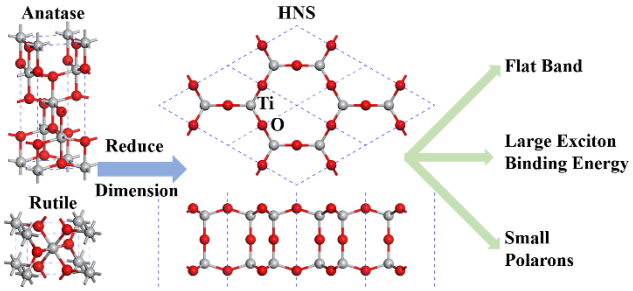
Anatase
HNS
Ti
O
Reduce
Dimension
Rutile
Flat Band
Large Exciton
Binding Energy
Small
Polarons